Materials & Design 225 (2023) 111526

Contents lists available at ScienceDirect

Materials & Design

journal homepage: www.elsevier.com/locate/matdes

γ-graphyne: A promising electron acceptor for organic photovoltaics

O.A. Stasyuk [a], A.J. Stasyuk [a,b,*], M. Solà [a,*], A.A. Voityuk [a,*]

[a] Institute of Computational Chemistry and Catalysis and Department of Chemistry University of Girona, C/ M. Aurèlia Capmany, 69, 17003 Girona, Spain
[b] Faculty of Chemistry, University of Warsaw, Pasteura 1, 02-093 Warsaw, Poland

HIGHLIGHTS

- electronic properties of **γ-graphyne** cluster models converge rapidly.
- electronic properties of **γ-graphyne** clusters have a low dependence on vacancy defects.
- **γ-graphyne** is an efficient electron acceptor (low LUMO and ability to delocalize excess charge).
- photoinduced electron transfer from electron donors to **γ-graphyne** is efficient and fast.

GRAPHICAL ABSTRACT

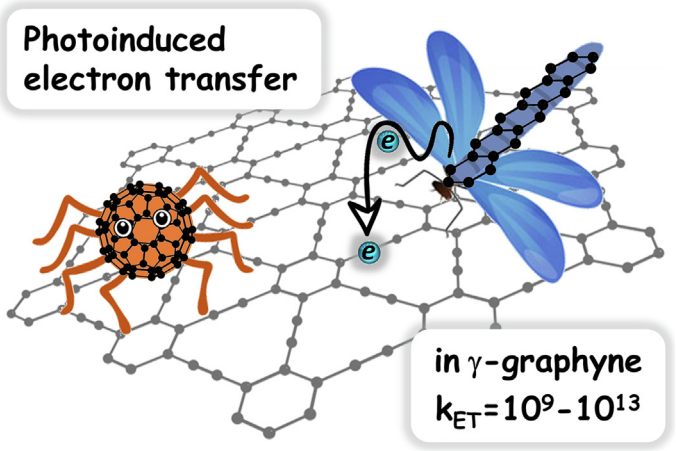

ARTICLE INFO

Article history:
Received 29 July 2022
Revised 19 December 2022
Accepted 19 December 2022
Available online 20 December 2022

Keywords:
Graphyne
Photoinduced electron transfer
Excited state
Electron acceptor
Cluster model

ABSTRACT

The search for new materials is constantly ongoing. Recently, a two-dimensional carbon allotrope , **γ-graphyne**, has been synthesized with a unified crystalline structure . Because of its low LUMO and excellent electron mobility, it appears to be a promising electron acceptor for photovoltaic applications. Here we report an analysis of the electronic properties of model van der Waals complexes of **γ-graphyne** with several partners of different electronic nature. We show that photoinduced electron transfer from electron-donating partners to **γ-graphyne** is favorable and occurs on nano to picosecond time scale. In contrast, electron transfer from **γ-graphyne** to strong electron acceptors is unlikely. Our results open perspectives for the future application of **γ-graphyne** in photovoltaic devices.

1. Introduction

Among the chemical elements, carbon holds the absolute champion for the number of reported allotropic forms. Diamond, graphite, and amorphous carbon have been known to mankind since ancient times. Two other allotropes of carbon, glassy carbon and lonsdaleite, were reported in the 1950s and 60s [1]. In 1980, carbon nano-onions were observed for the first time in vacuum-deposited amorphous carbon films [2]. However, a real breakthrough came in 1985 [3]. The buckminsterfullerene (C_{60}) detected by Kroto and co-workers made a sensation in chemistry and prompted many scientists to search for new carbon allotropes. In 1991, Iijima discovered carbon nanotubes (CNTs) [4], which, along with other findings, gave rise to a new branch of materials science,

* Corresponding authors.
E-mail addresses: antony.stasuk@gmail.com (A.J. Stasyuk), miquel.sola@udg.edu (M. Solà), alexander.voityuk@gmail.com (A.A. Voityuk).

https://doi.org/10.1016/j.matdes.2022.111526

nanoscience. Carbon nanofoam, a cluster-assembly of carbon atoms linked together in a loose three-dimensional network, was discovered by Rode and co-workers in the late 1990s [5]. 30 years later, the existence and structure of cyclo[18]carbon allotrope were experimentally confirmed by an IBM/Oxford team [6].

The most significant discovery of recent years is graphene, which consists of a single layer of carbon atoms arranged in a two-dimensional (2D) honeycomb lattice nanostructure [7]. Because of the exceptional properties of graphene such as optical transparency, large surface area, high Young's modulus, and excellent thermal conductivity, it has application in various fields including high-speed electronics, optical devices, energy generation and storage, hybrid materials, and chemical sensors [8–10]. Graphene, as a 2D sheet of sp^2-hybridized carbon, is currently a reference building block for other carbon allotropes: it can be stacked to form three-dimensional (3D) graphite, rolled into one-dimensional (1D) carbon nanotubes, and wrapped to zero-dimensional (0D) fullerenes. Thus, the discovery of graphene ushered in a new era of 2D materials. All of the carbon allotropes mentioned above consist of carbon atoms in the same hybridization state.

Two-dimensional materials similar to graphene, but composed of sp-hybridized carbons periodically integrated into an sp^2-hybridized carbon framework attract significant attention of scientists [11–14]. Graphynes, as a family of hybrid lattices, were first theoretically proposed by Baughman, Eckhardt, and Kertesz in 1987 [15]. In the last decade, the electronic, magnetic, and optical properties of graphyne and its analogs doped with heteroatoms have been intensively studied [16–19]. In 2010, Li *et al.* developed the first successful methodology for creating **γ-graphdiyne** films using the Glaser–Hay cross-coupling reaction with hexaethynylbenzene [20]. The proposed approach makes it possible to synthesize nanometer-scale graphdiyne and graphtetrayne, which lack long-range order [12,21]. In 2019, Cui and co-workers reported on a mechanochemical technique for obtaining **γ-graphyne** using benzene and CaC_2 [22]. Although a gram-scale **γ-graphyne** can be obtained using this approach, graphynes with long-range crystallinity over a large area remain elusive. Recently, Hu et al. reported **γ-graphyne** synthesis from 1,2,3,4,5,6-hexapropynylben zene and 1,2,3,4,5,6-hexakis[2-(4-hexylphenyl)ethynyl] benzene using Mo(VI) alkyne metathesis catalyst [23]. Various analytical methods indicate its excellent chemical and thermal stability. A wide-angle X-ray scattering characterization of the obtained **γ-graphyne** product suggests a unified crystalline structure. The synthesized **γ-graphyne** shows a broad absorption in the UV–vis and NIR regions. The material has a semiconductor band structure. Cyclic voltammetry and optical measurements suggest a band gap of 0.93 and 0.96 eV, respectively [23]. Previously, Chen *et al.* predicted that a sheet of sp-sp^2 hybridized carbons, as flat as **γ-graphyne**, should have greater carrier mobility (both electrons and holes) than a graphene sheet [24,25].

Taking into account the semiconductor nature of **γ-graphyne (γG)** as well as its promising transport properties [24], we explored its potential use in organic photovoltaics. Here we report an analysis of photoinduced electron transfer (PET) occurring in model van der Waals (vdW) complexes of **γ-graphyne** with typical electron donor and electron acceptor molecules used in organic solar cells. Our results clearly demonstrate that upon photoexcitation **γG** acts as a strong electron acceptor, and its complexes with electron donors show pronounced PET properties.

2. Computational methods

Geometry optimizations were carried out employing the BLYP [26,27] exchange–correlation functional with D3(BJ) empirical dispersion corrections [28,29] and Ahlrichs' def2-SVP basis set [30], using the resolution of identity approximation [31] as implemented in the ORCA 4.2.1 program [32]. Interaction energy, ΔE_{int}, and energy decomposition analysis (EDA) were calculated at the BLYP-D3(BJ)/TZ2P// BLYP-D3(BJ)/def2-SVP level using the Amsterdam Density Functional (ADF) program [33]. Electronic structure calculations were carried out with Gaussian 16 (rev. C01) [34] using the CAM-B3LYP [35] functional, because accurate prediction of charge transfer rates requires the use of range-separated functionals [36–38]. Besides, this functional shows the best performance for modeling charge transfer processes in fullerene-based complexes with a mean absolute percentage error of the logarithm of the charge transfer rate constant of 6.3 % [38]. Vertical excitation energies were calculated by time-dependent density-functional theory (TD-DFT) using the Tamm-Dancoff approximation (TDA). Electronic couplings were calculated by QChem 5.1 program [39]. To visualize molecular structures and frontier molecular orbitals, the Chemcraft 1.8 program [40] was used.

2.1. Analysis of excited states

Exciton delocalization and charge transfer in donor–acceptor complexes were quantitatively analyzed using the transition density [41–43]. The analysis was carried out in the more convenient Löwdin orthogonalized basis. The matrix $^{\lambda}\mathbf{C}$ of orthogonalized MO coefficients is obtained from the coefficients **C** in the original basis $^{\lambda}\mathbf{C} = \mathbf{S}^{1/2}\mathbf{C}$, where **S** is the atomic orbital overlap matrix. The transition density matrix T^{0i} for an excited state Φ_i^* constructed as a superposition of singly excited configurations (where an occupied MO ψ_j is replaced a virtual MO ψ_a) is computed,

$$T^{0i}_{\alpha\beta} = \sum_{ja} A_{j\to a} C^{\lambda}_{\alpha j} C^{\lambda}_{\beta a} \tag{1}$$

where $A_{j\to a}$ is the expansion coefficient and α and β are atomic orbitals.

A key quantity Ω(D,A) is determined by:

$$\Omega(D,A) = \sum_{\alpha\in D,\ \beta\in A} \left(T^{0i}_{\alpha\beta}\right)^2 \tag{2}$$

The weights of local excitations on donor (D) and acceptor (A) are Ω(D,D) and Ω(A,A). The weight of electron transfer configurations D → A and A → D is represented by Ω(D,A) and Ω(A,D), respectively. The index Δq, which describes charge separation and charge transfer between D and A, is

$$\Delta q(CS) = \sum \Omega(D,A) - \Omega(A,D) \tag{3}$$

$$\Delta q(CT) = \sum \Omega(D,A) + \Omega(A,D) \tag{4}$$

With this methodology, charge transfer (CT) states and local excited (LE) states) can be easily identified depending on the degree of the charge separation (CS).

2.2. Electron transfer rates

The rate of the nonadiabatic electron transfer (ET), k_{ET}, can be expressed in terms of the electronic coupling squared, V^2, and the Franck-Condon Weighted Density of states (FCWD):

$$k_{ET} = \frac{2\pi}{\hbar} V^2 (FCWD) \tag{5}$$

that accounts for the overlap of vibrational states of donor and acceptor and can be approximately estimated using the classical Marcus equation [44]:

$$(FCWD) = (4\pi\lambda kT)^{-1/2} \exp\left[-\left(\Delta G^0 + \lambda\right)^2 / 4\lambda kT\right] \tag{6}$$

where λ is the reorganization energy and ΔG^0 is the standard Gibbs energy change of the process. The electronic couplings between the LE, CT, and GS states calculated within TDA were calculated using the fragment charge difference (FCD) method [45,46].

The Marcus expression is derived for the high-temperature condition, $\hbar\omega_i \ll kT$, for all vibrational modes *i*. The semi-classical description of electron transfer (ET) [47] includes the effect of the quantum vibrational modes in an effective way, the solvent (low frequency) modes are treated classically, while a single high-frequency intramolecular mode $\omega_i, \hbar\omega_i \gg kT$, is described quantum mechanically. Because ET occurs normally from the lowest vibrational level of the initial state, the rate *k* can be expressed as a sum over all channels connecting the initial state with the vibrational quantum number n = 0 to manifold vibrational levels of the final state,

$$k = \sum_{n=0}^{\infty} k_{0\to n}, \text{ where } \quad k_{0\to n} = \frac{2\pi}{\hbar} V_{0\to n}^2 \frac{1}{\sqrt{4\pi\lambda_s kT}} \exp\left[-\frac{(\Delta G + n\hbar\omega_i + \lambda_s)^2}{4\lambda_s kT}\right] \tag{7}$$

with

$$V_{0\to n}^2 = V^2 \frac{S^n}{n!} \exp(-S) \tag{8}$$

An effective value of the Huang-Rhys factor *S* is estimated from the internal reorganization energy λ_i,

$$S = \lambda_i / \hbar\omega_i$$

2.3. Internal reorganization energy

The internal reorganization energy λ_i corresponds to the energy of structural changes when donor/acceptor goes from neutral-state geometries to charged-state geometries – cation and anion radicals, respectively.

$$\begin{aligned}
&\lambda_i = \lambda_i^1 + \lambda_i^2, \text{ where :}\\
&\lambda_i^1\left(\gamma G5^0 \to \gamma G5^-\right) = \tfrac{1}{2}\left[\left(\left(\gamma G5^0\right)_- - \left(\gamma G5^0\right)_0\right) + \left((\gamma G5^-)_0 - (\gamma G5^-)_-\right)\right]\\
&\lambda_i^2\left(Partner^0 \to Partner^+\right) = \tfrac{1}{2}\left[\left((Partner^0)_+ - (Partner^0)_0\right)\right.\\
&\left.+\left((Partner^+)_0 - (Partner^+)_+\right)\right]
\end{aligned} \tag{9}$$

where, as an example, $(\gamma G5^0)_-$ represents the energy of the anionic **γG5** calculated at the optimized geometry of the neutral **γG5**.

3. Results and discussion

3.1. Cluster model and electronic properties of γ-graphyne

Crystalline materials are mostly modeled by periodic treatment, which is quite efficient for computing the electronic structure of solids. This approach effectively accounts for long-range electrostatic effects and delocalized electronic coupling in metallic systems. However, its efficiency is severely reduced when periodic conditions are applied to local perturbations of the periodicity of the lattice (presence of defects, holes, inclusions, *etc.*), since large supercells should be treated to suppress spurious interactions between periodic images. For non-metallic systems, a cluster approach, which is focused on a finite-size model, can be applied. The reduction in system size opens the door to more accurate calculations of geometries, interaction energies, and electronic properties of the periodic systems. The cluster approach has been successfully applied to describe the electronic structure of graphene [48,49] and other semiconductors [50–52].

The choice of cluster size can significantly affect the calculation results. Thus, we generated several **γ-graphyne** clusters of different size (Fig. 1) and compared their electronic properties (Table 1).

As seen in Table 1, the dependence of electronic properties on the cluster size is not very significant. In particular, when the size increases by more than three times (from **γG1** to **γG5**), the HOMO energy changes by less than 0.1 eV. The LUMO energy varies more clearly, from −2.00 to −2.55 eV. The same is observed for the HOMO-LUMO (HL) gap, which decreases from −4.61 to −3.99 eV when moving from **γG1** to **γG5.** Table 1 demonstrates that the changes in orbital energies become smaller as the system size increases. In particular, the difference in the HL gap of **γG4** and **γG5** is found to be less than 0.1 eV. Changes in vertical ionization potential (VIP) and vertical electron affinity (VEA) values are found to be very similar to those observed for HOMO and LUMO energies, because long-range corrected DFT functionals (as CAM-B3LYP) approximately satisfy Koopmans' theorem both for HOMO and LUMO [53]. In particular, when moving from **γG1** to **γG5** cluster, VIP changes only by 0.1 eV, while VEA varies from 1.85 to 2.41 eV. As can be seen, VIP and VEA values slightly different from the corresponding orbital energies. In DFT, the Koopmans' theorem for a large molecular system states that the ionization energy of the *N*-electron system is equal to the negative arithmetic mean of the HOMO energy of this system and the energy of the LUMO of the (N-1)-electron system [54]. The calculated VIP and VES in Table 1 are in a good agreement with the predicted by the DFT-Koopmans' theorem values (Table S1, SI).

Wide-angle X-ray scattering and high-resolution transmission electron microscopy measurements in combination with solid state simulations revealed the ABC staggered interlayer stacking of the synthesized **γ-graphyne** [23]. The periodic calculations showed that the stacking leads to a band-gap decrease of 0.59 eV. The formation of the ABC type of stacking was also reported for graphene. The ABC graphene trilayer is a semiconductor with promising electronic properties [55,56]. In order to additionally verify the **γG5** model, we performed calculations for ABC-**γG5** stack (Fig. 2).

As seen from the presented data (Table 1 and Fig. 2), ABC stacking noticeably affects the orbital energies. The HL gap for ABC-**γG5** is 0.52 eV smaller than for **γG5**, which is in perfect agreement with the results obtained in the periodic calculation. The interlayer spacing in the ABC-**γG5** stack was found to be 3.26 Å, which is very close to previously reported 3.20 Å values [57]. It is important to note that the CAM-B3LYP functional significantly overestimates the HL gap compared the PBE functional (Table S2, SI). Considering the convergence of the electronic properties of **γ-graphyne** clusters with a gradual increase in their size, as well as a similar decrease in the HL gap with the formation of the ABC stack, it can be argued that the cluster approach is certainly applicable to **γ-graphyne**, and the system can be reliably described by the **γG5** cluster.

3.2. Defects in γ-graphyne

It is well known that electronic and mechanical properties of carbon materials with high atomic lattice perfection are extremely sensitive to structural defects. Vacancy defects in graphene have been shown to affect its electrical conductivity and other properties [58,59]. The influence of vacancy defects was also found for nanotubes. In particular, we recently reported that vacancies in phenine nanotube can strongly affect the rate of charge separation and charge recombination processes [60,61]. Similarly, the formation of structural defects in the manufacture of graphyne sheet is almost inevitable. Therefore, it seems necessary to carry out theo-

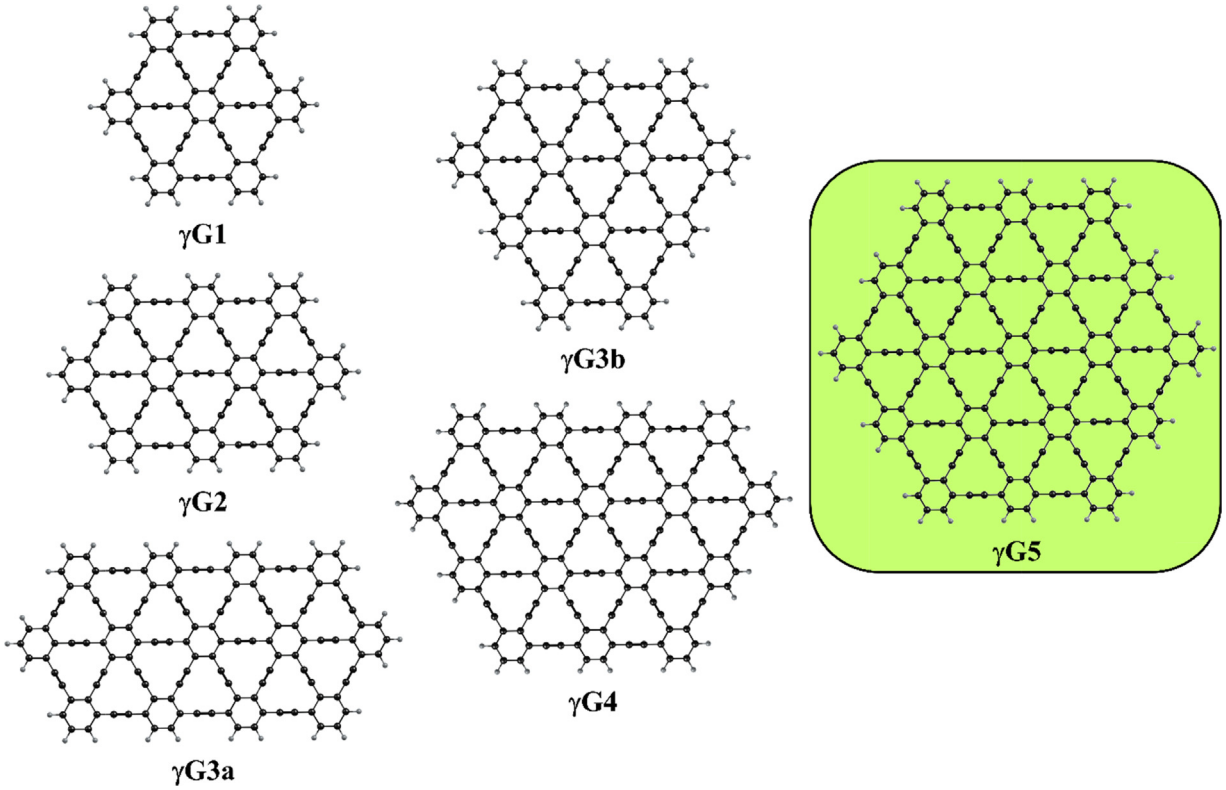

Fig. 1. Structure of the considered **γ-graphyne** clusters (**γG1** to **γG5**).

Table 1
HOMO and LUMO energies, HOMO-LUMO (HL) gap as well as vertical ionization potential (VIP) and electron affinity (VEA) values[a] (in eV) computed for **γ-graphyne** clusters of different size.

Cluster	Energy			VIP	VEA
	HOMO	LUMO	HL gap		
			γ-graphyne		
γG1	−6.603	−1.997	4.606	6.76	1.85
γG2	−6.556	−2.221	4.335	6.65	2.15
γG3a	−6.539	−2.351	4.188	6.61	2.31
γG3b	−6.539	−2.336	4.203	6.62	2.28
γG4	−6.535	−2.459	4.077	6.59	2.42
γG5	−6.533	−2.547	3.986	6.66	2.41
			ABC stack		
ABC-**γG5**	−6.053	−2.588	3.465	6.04	2.53

[a] VIP refers to the amount of energy required to remove one electron from the species to form a positive charge (VIP = E_{cation} - $E_{neutral}$). VEA is the amount of energy released when an electron attaches to a neutral species to form an anion (VEA = $E_{neutral}$ - E_{anion}). In both cases, the ion is in the same geometry as the optimized neutral system.

retical studies of the influence of these defects on the electronic properties of **γ-graphyne**.

We considered **γG5** with vacancy defects located at different nodes of the cluster. For comparison, we considered a giant $C_{222}H_{42}$ nanographene sheet [62] of a similar size (**Grphn** in Fig. 3). To simulate the defect, an 1,2,3,4,5,6-hexaethenylbenzene (HEB) unit in **γ-graphyne** and a coronene unit in nanographene were eliminated (Fig. 3). Open valence of carbon atoms were capped by hydrogen atoms and the models were considered in the closed-shell singlet ground state.

As seen in Fig. 3, the HOMO and LUMO energies of **γG5** and its analogues with defects are almost the same regardless of the defect location. The introduction of the defect causes a minor change in the HL gap. In the case of graphene, the defect causes dramatic changes in both HOMO and LUMO energies. The HL gap decreases by more than 1 eV. The effect depends on the defect position. In particular, the difference in the HL gap for **Grphn-D2** and **Grphn-D3** structures is 0.28 eV. The weak dependence of the electronic properties of **γ-graphyne** on the vacancy defect is especially important, because the sparse structure of **γ-graphyne** prevents conventional defect healing mechanism used for graphene nanostructures [63,64].

3.3. Van der Waals complexes

The high electron affinity of **γ-graphyne** and its promising electron transport properties suggest that the material can be involved into PET and be used in organic photovoltaics. To better understand this issue, we considered several vdW complexes formed by **γG5** and typical electron donor and electron acceptor molecules used in photovoltaics (Fig. 4). We selected fullerene C_{60}, perylenediimide (PDI), 11,11,12,12-tetracyano-9,10-anthraquinodimethane (TCAQ), and 5,10-dithiophene substituted naphtho[1,2-*c*:5,6-*c*']bis([1,2,5]thiadiazole) (NTDA) as acceptors and zinc-porphyrin (ZnP), zinc-phthalocyanine (ZnPc), 9,10-di(1,3-dithiol-2-ylidene)-9,10-dihydroanthracene (exTTF), 4,8-dithiophene substi-

Table 2
Distances (d in Å) between **γG5** plane and partner molecules, interaction energy (ΔE_{int}, kcal/mol), singlet excitation energy (E, eV), the degree of exciton localization (X) on **γG5**, the extent of charge separation (CT, e), as well as electron transfer parameters: Gibbs energy (ΔG^0, eV), electronic coupling ($|V_{ij}|$, eV), reorganization energy (λ, eV), electron transfer rate (k_{ET}, s^{-1}) and characteristic time (τ) for the studied vdW complexes.

	vdW complex **γG5** + Partner	d	ΔE_{int}[a]	Lowest LE (**γG5**)	CT state	ΔG^0 [b]	$\|V_{ij}\|$	λ	k_{ET}	τ[c]
1	**γG5** + C_{60}	6.312[d]	−18.04	E = 2.087 X = 0.981	E = 3.071 CT = 0.903[f]	0.984	$6.98 \cdot 10^{-3}$	0.127	[n/a]	[n/a]
2	**γG5** + PDI	3.216	−49.38	E = 2.077 X = 0.930	E = 2.952 CT = 0.820[f]	0.875	$3.45 \cdot 10^{-2}$	0.183	[n/a]	[n/a]
3	**γG5** + TCAQ	3.594[e]	−47.57	E = 2.085 X = 0.972	E = 2.995 CT = 0.857[f]	0.870	$3.83 \cdot 10^{-2}$	0.207	[n/a]	[n/a]
4	**γG5** + NTDA	3.255	−26.45	E = 2.074 X = 0.955	E = 3.070 CT = 0.853[f]	0.996	$2.65 \cdot 10^{-2}$	0.155	[n/a]	[n/a]
					E = 2.173 CT = 0.795[g]	0.099	$3.84 \cdot 10^{-2}$	0.152	$1.04 \cdot 10^{10}$	0.09 ns
5	**γG5** + ZnP	3.197	−39.91	E = 2.089 X = 0.877	E = 1.974 CT = 0.901[g]	−0.115	$1.88 \cdot 10^{-2}$	0.101	$9.96 \cdot 10^{9}$	0.10 ns
6	**γG5** + ZnPc	3.216	−62.48	E = 2.090 X = 0.941	E = 1.526 CT = 0.939[g]	−0.564	$1.05 \cdot 10^{-2}$	0.104	$5.32 \cdot 10^{10}$	18.8 ps
7	**γG5** + ExTTF	3.586[e]	−24.49	E = 2.091 X = 0.961	E = 1.722 CT = 0.984[g]	−0.369	$3.99 \cdot 10^{-3}$	0.211	$1.32 \cdot 10^{11}$	7.6 ps
8	**γG5** + BDT	3.335[e]	−25.59	E = 2.092 X = 0.900	E = 1.923 CT = 0.875[g]	−0.169	$3.04 \cdot 10^{-2}$	0.312	$1.15 \cdot 10^{13}$	0.09 ps
9	**γG5** + PNTCN	3.242	−38.83	E = 2.104 X = 0.945	E = 1.706 CT = 0.905[g]	−0.398	$1.30 \cdot 10^{-2}$	0.099	$1.78 \cdot 10^{12}$	0.6 ps

[a] $\Delta E_{int} = E_{complex} - (E_{\gamma G5} + E_{partner})$.
[b] Gibbs energy difference between the lowest LE and CT states.
[c] characteristic time defined as the reciprocal of the rate constant $\tau = (k_{ET})^{-1}$.
[d] distance between center of C_{60} fullerene and **γG5** plane.
[e] distance between central benzene ring of partner molecule and **γG5** plane.
[f] electron transfer from **γG5** to the partner.
[g] electron transfer from the partner to **γG5**.

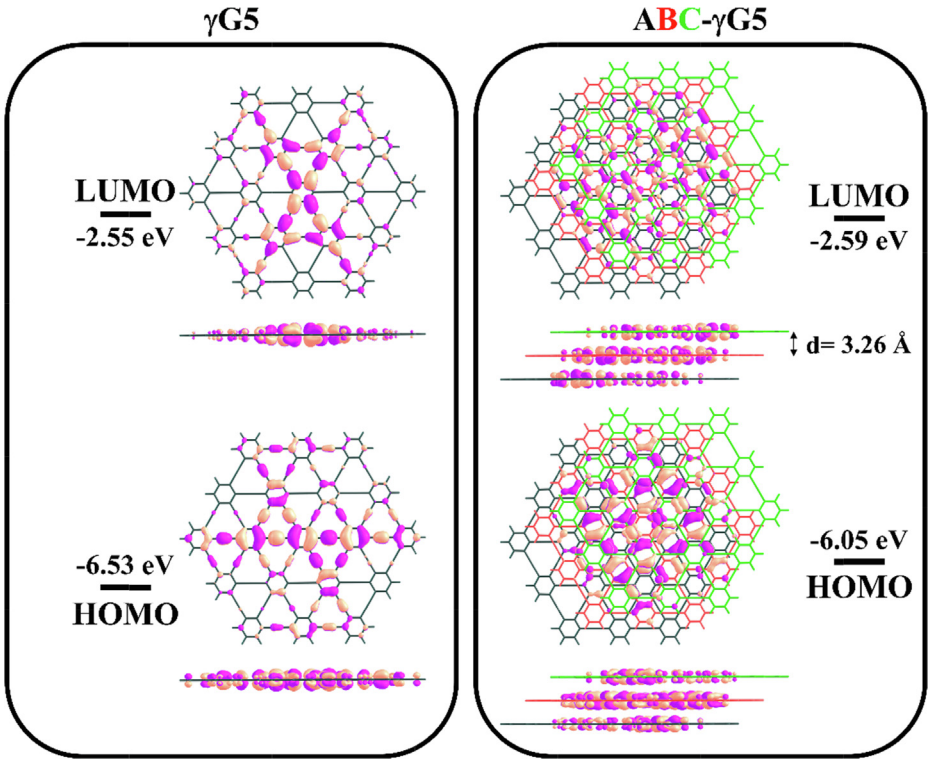

Fig. 2. Structure and HOMO/LUMO energies of **γG5** and ABC-**γG5** stack. Distance between layers in ABC-**γG5** stack is denoted by **d** and is equal to 3.26 Å.

tuted benzo[1,2-*b*:4,5-*b*']dithiophene (BDT), and pentacene (PNTCN) as electron donors.

Geometries of the vdW complexes were optimized using the BLYP-D3(BJ)/def2-SVP level of theory. Several possible conformers were analyzed. The structures of the most stable complexes are given in Figure S1, SI. The distances between the plane of **γG5** and partner molecules and interaction energy (ΔE_{int}) between them are listed in Table 2. Depending on the geometry of the partner, the systems of interest are divided into 2 groups: 1) with a strong noncovalent binding (−38 ÷ −62 kcal/mol) observed in the

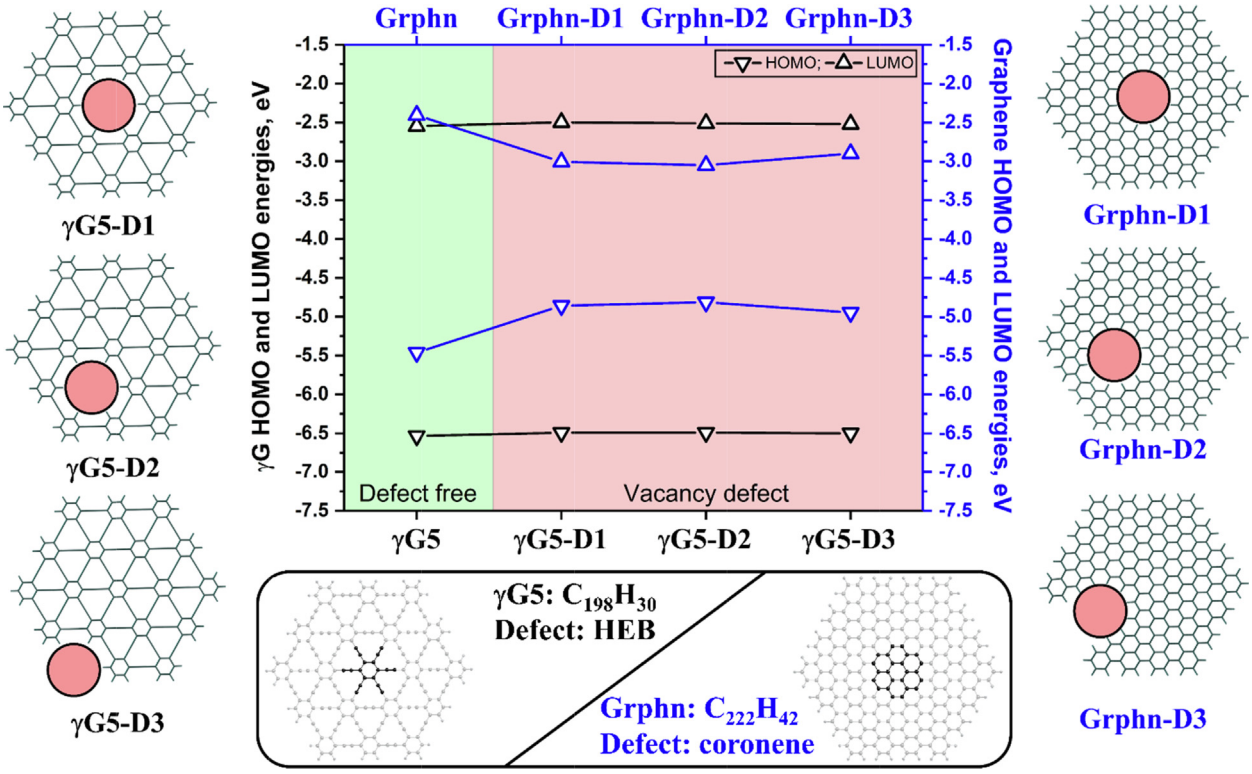

Fig. 3. Structure and HOMO/LUMO energies of γ-**graphyne** and nanographene with vacancy defects (depicted as a black moiety). The red circle indicates the defects caused by missing HEB or coronene units. (For interpretation of the references to colour in this figure legend, the reader is referred to the web version of this article).

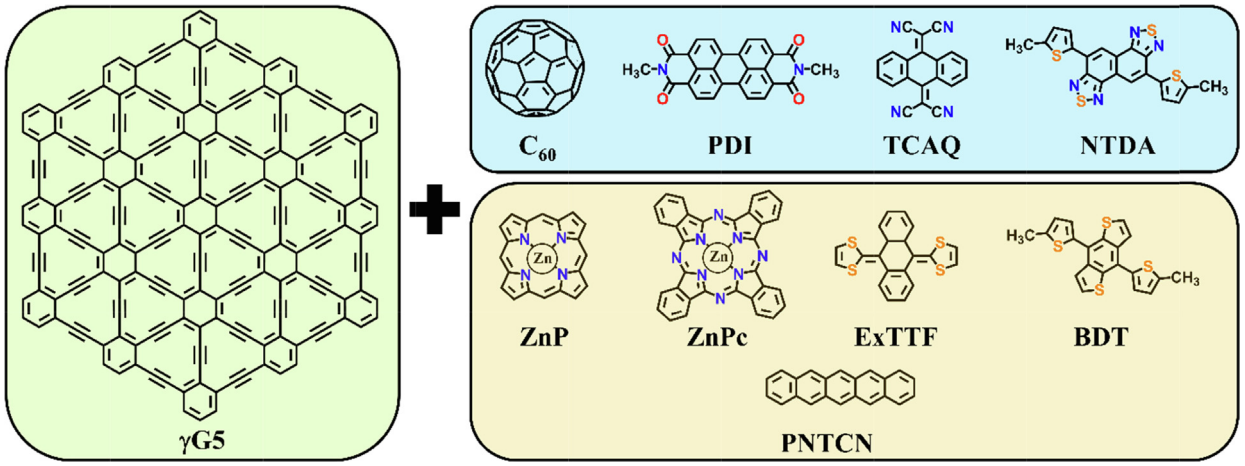

Fig. 4. Electron acceptor (top) and electron donor (bottom) partners of **γG5** in the van der Waals complexes.

complexes with planar molecules, such as PDI, NTDA, ZnP, ZnPc, and PNTCN; and 2) with a weak interaction energy (−18 ÷ −26 kcal/mol) found in the complexes with non-planar partners, such as C_{60}, TCAQ, ExTTF, and BDT. For comparison, the interaction of C_{60} with graphene was found to be −15.68 kcal/mol at the PBE/6-31G(d,p) level [65], but self-organization of fullerene molecules on graphene has been established experimentally [66]. The weak interaction energy with non-planar partners is in a perfect agreement with the distance between **γG5** plane and the partner molecules. Analysis of the partner structures revealed that upon the complex formation none of the planar molecules demonstrates out-of-plane deviations. However, the formation of the vdW complexes with non-planar TCAQ, ExTTF, and BDT molecules leads to their partial planarization compared to their isolated form. Comparison of geometrical changes for the denoted molecules is given in Figure S2, SI.

The nature of non-covalent interactions was investigated by the Morokuma-like energy decomposition analysis (EDA) [67,68], which decomposes the total interaction energy into four components (Pauli repulsion, electrostatic interactions, orbital interactions, and D3(BJ) dispersion correction). For an easier analysis, we will discuss the relative contributions of the different attractive interactions ($\Delta E_{elstat} + \Delta E_{oi} + \Delta E_{disp}$). The dispersion was found to be a dominant attractive term in all complexes, with a contribution of 53 to 66 %. The second largest term is the electrostatic attraction accounting for 21 to 31 %. The orbital interaction provides 11–16 % of the total stabilizing energy. The EDA results are shown in Table S3, SI.

3.4. Singlet excited states and electron transfer rates

To describe the excited-state properties of the vdW complexes, all systems were divided into 2 fragments: **γ-graphyne** and partner molecule. The electron density distribution was analyzed for the 50 lowest singlet excited states. Three types of the excited states were identified: (1) locally excited (LE) states, in which the exciton is mainly localized either on **γ-graphyne** ($LE^{\gamma G5}$) or the partner molecule ($LE^{Partner}$) and intermolecular charge transfer is small (CS less than 0.1 ***e***); (2) charge transfer (CT) states (CS greater than 0.8 ***e***) showing a significant charge separation; and (3) mixed states, where both LE and CT states contribute substantially (0.1 ***e*** < CS < 0.8 ***e***).

The behavior of the vdW complexes in the excited state depends strongly on the properties of the partner molecule. If the partner is a strong electron donor, the lowest excited state is a CT state, in which electron density is transferred from the partner molecule to **γG5.** Its energy is about 1.5–2.0 eV (Table 2). However, if the partner is an electron acceptor, the lowest excited state corresponds to $LE^{\gamma G5}$ and is found at *ca.* 2.08 eV. The CT states with electron transfer from **γG5** to the partner molecule is higher in energy by almost 1 eV. We note that the **γG5** + NTDA complex differs from other systems. The electron-accepting properties of NTDA were found to be close to those of **γG5**. As a result, two types of CT states (**γG5** → NTDA and NTDA → **γG5**) have similar energies.

The **γG5** unit is characterized by a strong light absorption in the green–blue region and a very low internal reorganization energy, which determines its ability to both charge separation and charge transport. Simulated absorption spectra of all studied complexes are presented in Figure S3 in SI. Table 2 shows selected excited-state properties of the studied vdW complexes. The detailed analysis of the excited states is provided in Table S2, SI.

The non-adiabatic electron transfer rate, k_{ET}, was estimated using the semi-classical approach (for details see the SI) proposed by Ulstrup and Jortner [47]. The results obtained by this methodology are in a good agreement with experimental data for noncovalent complexes of ZnP–[10]CPP and doubly curved nanographene with C_{60} [69,70]. The predicted internal reorganization energy of **γG5** is very small, which correlates well with the experimentally observed high carrier mobility [23].

The photoinduced electron transfer from **γG5** to the electron acceptor (e.g. C_{60}, PDI, and TCAQ) is characterized by positive Gibbs energy, which makes this process highly unfavorable. As noted above, two types of CT are possible in **γG5** + NTDA (**γG5** → NTDA and NTDA → **γG5**). When NTDA acts as an electron acceptor, the charge transfer is not feasible due to the positive Gibbs energy. In contrast, when NTDA is an electron donor, the reaction Gibbs energy is close to zero and reaction occurs in the normal Marcus region. The assignment of the ET process to the normal or inverted region occurs in accordance with the classical Marcus theory [44]. In the normal region, k_{ET} increases with increasing $-\Delta G^0$ until the reorganization energy matches the driving force ($-\Delta G^0 = \lambda$). Within the inverted region, k_{ET} decreases with further increasing $-\Delta G^0$. For other complexes with electron-donating partners (ZnP, ZnPc, ExTTF, BDT, and PNTCN), the Gibbs energy is negative and charge separation occurs on the nanosecond to sub-picosecond time scale (Table 2). For the complexes with ZnPc, ExTTF, and PNTCN, $-\Delta G^0 > \lambda$, which corresponds to the inverted region.

4. Conclusions

In this work, we studied non-covalent complexes of **γ-graphyne** with typical electron donor and acceptor molecules. Our results demonstrate that **γ-graphyne** is an efficient electron acceptor due to its low LUMO and its ability to delocalize an excess of charge. Moreover, its electronic properties are not sensitive to vacancy defects in the structure. The TD-DFT results indicate that photoinduced electron transfer from electron-donating partners to **γG5** is quite efficient and fast, whereas electron transfer from **γG5** to an electron-accepting molecule is energetically unfavorable. Overall, our results suggest that **γ-graphyne** is a promising material for organic photovoltaics.

CRediT authorship contribution statement

O.A. Stasyuk: Investigation, Formal analysis, Writing – original draft, Writing – review & editing. **A.J. Stasyuk:** Supervision, Investigation, Formal analysis, Writing – original draft, Writing – review & editing. **M. Solà:** Supervision, Writing – review & editing, Funding acquisition. **A.A. Voityuk:** Supervision, Writing – review & editing.

Data availability

All data needed to reproduce the results are included in the Supporting Information

Declaration of Competing Interest

The authors declare that they have no known competing financial interests or personal relationships that could have appeared to influence the work reported in this paper.

Acknowledgements

We are grateful for financial support from the Spanish Ministerio de Ciencia e Innovación (Network RED2018-102815-T, project PID2020-13711 GB-I00, and Juan de la Cierva contract IJC2019-039846-I to A.J.S.), the Catalan DIUE (2017SGR39) and the University of Girona (POSTDOC-UdG 2021/31 to O.A.S.). A.J.S. gratefully acknowledge Poland's high-performance computing infrastructure PLGrid (HPC Centers: ACK Cyfronet AGH) for providing computer facilities and support within computational grant no. PLG/2022/015756.

Appendix A. Supplementary data

Supplementary data to this article can be found online at https://doi.org/10.1016/j.matdes.2022.111526.

References

[1] V. Uskoković, A historical review of glassy carbon: Synthesis, structure, properties and applications, Carbon Trends 5 (2021) 100116.
[2] S. Iijima, Direct observation of the tetrahedral bonding in graphitized carbon black by high resolution electron microscopy, J. Cryst. Growth 50 (1980) 675–683.
[3] H.W. Kroto, J.R. Heath, S.C. O'Brien, R.F. Curl, R.E. Smalley, C_{60}: Buckminsterfullerene, Nature 318 (1985) 162–163.
[4] S. Iijima, Helical microtubules of graphitic carbon, Nature 354 (1991) 56–58.
[5] A.V. Rode, S.T. Hyde, E.G. Gamaly, R.G. Elliman, D.R. McKenzie, S. Bulcock, Structural analysis of a carbon foam formed by high pulse-rate laser ablation, Appl. Phys. A: Mater. Sci. Process. 69 (1999) S755–S758.
[6] K. Kaiser, L.M. Scriven, F. Schulz, P. Gawel, L. Gross, H.L. Anderson, An sp-hybridized molecular carbon allotrope, cyclo[18]carbon, Science 365 (2019) 1299–1301.
[7] A.K. Geim, K.S. Novoselov, The rise of graphene, Nat. Mater. 6 (2007) 183–191.
[8] Y. Zhu, S. Murali, W. Cai, X. Li, J.W. Suk, J.R. Potts, R.S. Ruoff, Graphene and Graphene Oxide: Synthesis, Properties, and Applications, Adv. Mater. 22 (2010) 3906–3924.
[9] F. Bonaccorso, Z. Sun, T. Hasan, A.C. Ferrari, Graphene photonics and optoelectronics, Nat. Photonics 4 (9) (2010) 611–622.
[10] V. Georgakilas, J.N. Tiwari, K.C. Kemp, J.A. Perman, A.B. Bourlinos, K.S. Kim, R. Zboril, Noncovalent Functionalization of Graphene and Graphene Oxide for Energy Materials, Biosensing, Catalytic, and Biomedical Applications, Chem. Rev. 116 (2016) 5464–5519.

[11] X. Gao, H.B. Liu, D. Wang, J. Zhang, Graphdiyne: synthesis, properties, and applications, Chem. Soc. Rev. 48 (2019) 908–936.
[12] Y. Li, L. Xu, H. Liu, Y. Li, Graphdiyne and graphyne: from theoretical predictions to practical construction, Chem. Soc. Rev. 43 (2014) 2572–2586.
[13] H. Tang, C.M. Hessel, J. Wang, N. Yang, R. Yu, H. Zhao, D. Wang, Two-dimensional carbon leading to new photoconversion processes, Chem. Soc. Rev. 43 (2014) 4281–4299.
[14] J. Deb, R. Mondal, U. Sarkar, H. Sadeghi, Thermoelectric Properties of Pristine Graphyne and the BN-Doped Graphyne Family, ACS Omega 6 (2021) 20149–20157.
[15] R.H. Baughman, H. Eckhardt, M. Kertesz, Structure-property predictions for new planar forms of carbon: Layered phases containing sp^2 and sp atoms, J. Chem. Phys. 87 (1987) 6687–6699.
[16] B. Bhattacharya, J. Deb, U. Sarkar, Boron-phosphorous doped graphyne: A near-infrared light absorber, AIP Adv. 9 (2019) 095031.
[17] B. Bhattacharya, U. Sarkar, The Effect of Boron and Nitrogen Doping in Electronic, Magnetic, and Optical Properties of Graphyne, J. Phys. Chem. C 120 (2016) 26793–26806.
[18] B. Bhattacharya, U. Sarkar, N. Seriani, Electronic Properties of Homo- and Heterobilayer Graphyne: The Idea of a Nanocapacitor, J. Phys. Chem. C 120 (2016) 26579–26587.
[19] J. Deb, B. Bhattacharya, N.B. Singh, U. Sarkar, First principle study of adsorption of boron-halogenated system on pristine graphyne, Struct. Chem. 27 (2016) 1221–1227.
[20] G. Li, Y. Li, H. Liu, Y. Guo, Y. Li, D. Zhu, Architecture of graphdiyne nanoscale films, Chem. Commun. 46 (2010) 3256–3258.
[21] C. Huang, Y. Li, N. Wang, Y. Xue, Z. Zuo, H. Liu, Y. Li, Progress in Research into 2D Graphdiyne-Based Materials, Chem. Rev. 118 (2018) 7744–7803.
[22] Q. Li, C. Yang, L. Wu, H. Wang, X. Cui, Converting benzene into γ-graphyne and its enhanced electrochemical oxygen evolution performance, J. Mater. Chem. A 7 (2019) 5981–5990.
[23] Y. Hu, C. Wu, Q. Pan, Y. Jin, R. Lyu, V. Martinez, S. Huang, J. Wu, L.J. Wayment, N. A. Clark, M.B. Raschke, Y. Zhao, W. Zhang, Synthesis of γ-graphyne using dynamic covalent chemistry, Nat. Synth. 1 (2022) 449–454.
[24] J. Chen, J. Xi, D. Wang, Z. Shuai, Carrier Mobility in Graphyne Should Be Even Larger than That in Graphene: A Theoretical Prediction, J. Phys. Chem. Lett. 4 (2013) 1443–1448.
[25] J. Kang, J. Li, F. Wu, S.-S. Li, J.-B. Xia, Elastic, Electronic, and Optical Properties of Two-Dimensional Graphyne Sheet, J. Phys. Chem. C 115 (2011) 20466–20470.
[26] A.D. Becke, Density-functional exchange-energy approximation with correct asymptotic behavior, Phys. Rev. A 38 (1988) 3098–3100.
[27] C. Lee, W. Yang, R.G. Parr, Development of the Colle-Salvetti correlation-energy formula into a functional of the electron density, Phys. Rev. B 37 (1988) 785–789.
[28] S. Grimme, S. Ehrlich, L. Goerigk, Effect of the damping function in dispersion corrected density functional theory, J. Comput. Chem. 32 (2011) 1456–1465.
[29] S. Grimme, J. Antony, S. Ehrlich, H. Krieg, A consistent and accurate ab initio parametrization of density functional dispersion correction (DFT-D) for the 94 elements H-Pu, J. Chem. Phys. 132 (2010) 154104.
[30] F. Weigend, R. Ahlrichs, Balanced basis sets of split valence, triple zeta valence and quadruple zeta valence quality for H to Rn: Design and assessment of accuracy, Phys. Chem. Chem. Phys. 7 (2005) 3297–3305.
[31] K. Eichkorn, O. Treutler, H. Öhm, M. Häser, R. Ahlrichs, Auxiliary basis sets to approximate Coulomb potentials, Chem. Phys. Lett. 240 (1995) 283–290.
[32] F. Neese, Software update: the ORCA program system, version 4.0, WIREs Comput, Mol. Sci. 8 (2018) e1327.
[33] ADF 2017, SCM, Theoretical Chemistry, Vrije Universiteit, Amsterdam, The Netherlands, http://www.scm.com.
[34] Gaussian 16, Revision C.01, M. J. Frisch, G. W. Trucks, H. B. Schlegel, G. E. Scuseria, M. A. Robb, J. R. Cheeseman, G. Scalmani, V. Barone, G. A. Petersson, H. Nakatsuji, X. Li, M. Caricato, A. V. Marenich, J. Bloino, B. G. Janesko, R. Gomperts, B. Mennucci, H. P. Hratchian, J. V. Ortiz, A. F. Izmaylov, J. L. Sonnenberg, D. Williams-Young, F. Ding, F. Lipparini, F. Egidi, J. Goings, B. Peng, A. Petrone, T. Henderson, D. Ranasinghe, V. G. Zakrzewski, J. Gao, N. Rega, G. Zheng, W. Liang, M. Hada, M. Ehara, K. Toyota, R. Fukuda, J. Hasegawa, M. Ishida, T. Nakajima, Y. Honda, O. Kitao, H. Nakai, T. Vreven, K. Throssell, J. A. Montgomery, Jr., J. E. Peralta, F. Ogliaro, M. J. Bearpark, J. J. Heyd, E. N. Brothers, K. N. Kudin, V. N. Staroverov, T. A. Keith, R. Kobayashi, J. Normand, K. Raghavachari, A. P. Rendell, J. C. Burant, S. S. Iyengar, J. Tomasi, M. Cossi, J. M. Millam, M. Klene, C. Adamo, R. Cammi, J. W. Ochterski, R. L. Martin, K. Morokuma, O. Farkas, J. B. Foresman, and D. J. Fox, Gaussian, Inc., Wallingford CT, 2016.
[35] T. Yanai, D.P. Tew, N.C. Handy, A new hybrid exchange–correlation functional using the Coulomb-attenuating method (CAM-B3LYP), Chem. Phys. Lett. 393 (2004) 51–57.
[36] B.M. Wong, T.H. Hsieh, Optoelectronic and Excitonic Properties of Oligoacenes: Substantial Improvements from Range-Separated Time-Dependent Density Functional Theory, J. Chem. Theory Comput. 6 (2010) 3704–3712.
[37] Y. Imamura, R. Kobayashi, H. Nakai, Construction of orbital-specific hybrid functional by imposing the linearity condition for orbital energies in density functional theory, Procedia Comput. Sci. 4 (2011) 1151–1156.
[38] P. Besalú-Sala, A.A. Voityuk, J.M. Luis, M. Solà, Evaluation of charge-transfer rates in fullerene-based donor–acceptor dyads with different density functional approximations, Phys. Chem. Chem. Phys. 23 (2021) 5376–5384.
[39] Y. Shao, Z. Gan, E. Epifanovsky, A.T.B. Gilbert, M. Wormit, J. Kussmann, A.W. Lange, A. Behn, J. Deng, X. Feng, D. Ghosh, M. Goldey, P.R. Horn, L.D. Jacobson, I. Kaliman, R.Z. Khaliullin, T. Kuś, A. Landau, J. Liu, E.I. Proynov, Y.M. Rhee, R.M. Richard, M.A. Rohrdanz, R.P. Steele, E.J. Sundstrom, H.L. Woodcock, P.M. Zimmerman, D. Zuev, B. Albrecht, E. Alguire, B. Austin, G.J.O. Beran, Y.A. Bernard, E. Berquist, K. Brandhorst, K.B. Bravaya, S.T. Brown, D. Casanova, C.-M. Chang, Y. Chen, S.H. Chien, K.D. Closser, D.L. Crittenden, M. Diedenhofen, R.A. DiStasio, H. Do, A.D. Dutoi, R.G. Edgar, S. Fatehi, L. Fusti-Molnar, A.n. Ghysels, A. Golubeva-Zadorozhnaya, J. Gomes, M.W.D. Hanson-Heine, P.H.P. Harbach, A. W. Hauser, E.G. Hohenstein, Z.C. Holden, T.-C. Jagau, H. Ji, B. Kaduk, K. Khistyaev, J. Kim, J. Kim, R.A. King, P. Klunzinger, D. Kosenkov, T. Kowalczyk, C. M. Krauter, K.U. Lao, A.D. Laurent, K.V. Lawler, S.V. Levchenko, C.Y. Lin, F. Liu, E. Livshits, R.C. Lochan, A. Luenser, P. Manohar, S.F. Manzer, S.-P. Mao, N. Mardirossian, A.V. Marenich, S.A. Maurer, N.J. Mayhall, E. Neuscamman, C.M. Oana, R. Olivares-Amaya, D.P. O'Neill, J.A. Parkhill, T.M. Perrine, R. Peverati, A. Prociuk, D.R. Rehn, E. Rosta, N.J. Russ, S.M. Sharada, S. Sharma, D.W. Small, A. Sodt, T. Stein, D. Stück, Y.-C. Su, A.J.W. Thom, T. Tsuchimochi, V. Vanovschi, L. Vogt, O. Vydrov, T. Wang, M.A. Watson, J. Wenzel, A. White, C.F. Williams, J. Yang, S. Yeganeh, S.R. Yost, Z.-Q. You, I.Y. Zhang, X. Zhang, Y. Zhao, B.R. Brooks, G.K.L. Chan, D.M. Chipman, C.J. Cramer, W.A. Goddard, M.S. Gordon, W.J. Hehre, A. Klamt, H.F. Schaefer, M.W. Schmidt, C.D. Sherrill, D.G. Truhlar, A. Warshel, X. Xu, A. Aspuru-Guzik, R. Baer, A.T. Bell, N.A. Besley, J.-D. Chai, A. Dreuw, B.D. Dunietz, T.R. Furlani, S.R. Gwaltney, C.-P. Hsu, Y. Jung, J. Kong, D.S. Lambrecht, WanZhen Liang, C. Ochsenfeld, V.A. Rassolov, L.V. Slipchenko, J.E. Subotnik, T. Van Voorhis, J.M. Herbert, A.I. Krylov, P.M.W. Gill, M. Head-Gordon, Advances in molecular quantum chemistry contained in the Q-Chem 4 program package, Mol. Phys. 113 (2015) 184–215.
[40] G. A. Zhurko, Chemcraft 1.80 (build 523b) - graphical program for visualization of quantum chemistry computations. (https://chemcraftprog.com).
[41] F. Plasser, H. Lischka, Analysis of Excitonic and Charge Transfer Interactions from Quantum Chemical Calculations, J. Chem. Theory Comput. 8 (2012) 2777–2789.
[42] F. Plasser, S.A. Bäppler, M. Wormit, A. Dreuw, New tools for the systematic analysis and visualization of electronic excitations. II. Applications, J. Chem. Phys. 141 (2014) 024107.
[43] A.V. Luzanov, O.A. Zhikol, Electron invariants and excited state structural analysis for electronic transitions within CIS, RPA, and TDDFT models, Int. J. Quantum Chem. 110 (2010) 902–924.
[44] R.A. Marcus, N. Sutin, Electron transfers in chemistry and biology, Biochim. Biophys. Acta, Rev. Bioenerg. 811 (1985) 265–322.
[45] A.A. Voityuk, N. Rösch, Fragment charge difference method for estimating donor–acceptor electronic coupling: Application to DNA π-stacks, J. Chem. Phys. 117 (2002) 5607–5616.
[46] A.A. Voityuk, Electronic coupling for charge transfer in donor–bridge–acceptor systems. Performance of the two-state FCD model, Phys. Chem. Chem. Phys. 14 (2012) 13789–13793.
[47] J. Ulstrup, J. Jortner, The effect of intramolecular quantum modes on free energy relationships for electron transfer reactions, J. Chem. Phys. 63 (1975) 4358–4368.
[48] M. Pykal, P. Jurečka, F. Karlický, M. Otyepka, Modelling of graphene functionalization, Phys. Chem. Chem. Phys. 18 (2016) 6351–6372.
[49] K. Larson, A. Clark, A. Appel, Q. Dai, H. He, S. Zygmunt, Surface-dependence of interfacial binding strength between zinc oxide and graphene, RSC Adv. 5 (2015) 65719–65724.
[50] N. Hansen, T. Kerber, J. Sauer, A.T. Bell, F.J. Keil, Quantum Chemical Modeling of Benzene Ethylation over H-ZSM-5 Approaching Chemical Accuracy: A Hybrid MP2:DFT Study, J. Am. Chem. Soc. 132 (2010) 11525–11538.
[51] K. Raghavachari, M.D. Halls, Quantum chemical studies of semiconductor surface chemistry using cluster models, Mol. Phys. 102 (2004) 381–393.
[52] J.A. Keith, A.B. Muñoz-García, M. Lessio, E.A. Carter, Cluster Models for Studying CO_2 Reduction on Semiconductor Photoelectrodes, Top. Catal. 58 (2015) 46–56.
[53] T. Tsuneda, J.-W. Song, S. Suzuki, K. Hirao, On Koopmans' theorem in density functional theory, J. Chem. Phys. 133 (2010) 174101.
[54] J.i. Luo, Z.Q. Xue, W.M. Liu, J.L. Wu, Z.Q. Yang, Koopmans' Theorem for Large Molecular Systems within Density Functional Theory, J. Phys. Chem. A 110 (2006) 12005–12009.
[55] Y. Shan, Y. Li, D. Huang, Q. Tong, W. Yao, W.-T. Liu, S. Wu, Stacking symmetry governed second harmonic generation in graphene trilayers, Sci. Adv. 4 (2018) eaat0074.
[56] Z. Gao, S. Wang, J. Berry, Q. Zhang, J. Gebhardt, W.M. Parkin, J. Avila, H. Yi, C. Chen, S. Hurtado-Parra, M. Drndić, A.M. Rappe, D.J. Srolovitz, J.M. Kikkawa, Z. Luo, M.C. Asensio, F. Wang, A.T.C. Johnson, Large-area epitaxial growth of curvature-stabilized ABC trilayer graphene, Nat. Commun. 11 (2020) 546.
[57] S.W. Cranford, M.J. Buehler, Mechanical properties of graphyne, Carbon 49 (2011) 4111–4121.
[58] F. Banhart, J. Kotakoski, A.V. Krasheninnikov, Structural Defects in Graphene, ACS Nano 5 (2011) 26–41.
[59] G. Yang, L. Li, W.B. Lee, M.C. Ng, Structure of graphene and its disorders: a review, Sci. Technol. Adv. Mater. 19 (2018) 613–648.
[60] A.J. Stasyuk, O.A. Stasyuk, M. Solà, A.A. Voityuk, Photoinduced electron transfer in nanotube⊃C70 inclusion complexes: phenine vs. nanographene nanotubes, Chem. Commun. 56 (2020) 12624–12627.
[61] O.A. Stasyuk, A.J. Stasyuk, M. Solà, A.A. Voityuk, How Do Defects in Carbon Nanostructures Regulate the Photoinduced Electron Transfer Processes?, The Case of Phenine Nanotubes, ChemPhysChem 22 (2021) 1178–1186

[62] C.D. Simpson, J.D. Brand, A.J. Berresheim, L. Przybilla, H.J. Räder, K. Müllen, Synthesis of a Giant 222 Carbon Graphite Sheet, Chem. Eur. J. 8 (2002) 1424–1429.
[63] G. Li, P. Xiao, S. Hou, Y. Huang, Graphene based self-healing materials, Carbon 146 (2019) 371–387.
[64] L. Liu, M. Qing, Y. Wang, S. Chen, Defects in Graphene: Generation, Healing, and Their Effects on the Properties of Graphene: A Review, J. Mater. Sci. Technol. 31 (2015) 599–606.
[65] D. Cortes-Arriagada, L. Sanhueza, A. Bautista-Hernandez, M. Salazar-Villanueva, E. Chigo Anota, Chemical and Physical Viewpoints About the Bonding in Fullerene-Graphene Hybrid Materials: Interaction on Pristine and Fe-Doped Graphene, J. Phys. Chem. C 123 (2019) 24209–24219.
[66] Y. Li, X. Liu, C. Chen, J. Duchamp, R. Huang, T.-F. Chung, M. Young, T. Chalal, Y.P. Chen, J.R. Heflin, H.C. Dorn, C. Tao, Differences in self-assembly of spherical C_{60} and planar PTCDA on rippled graphene surfaces, Carbon 145 (2019) 549–555.
[67] K. Morokuma, Why do molecules interact? The origin of electron donor-acceptor complexes, hydrogen bonding and proton affinity, Acc. Chem. Res. 10 (1977) 294–300.
[68] T. Ziegler, A. Rauk, On the calculation of bonding energies by the Hartree Fock Slater method, Theor. Chim. Acta 46 (1977) 1–10.
[69] A.J. Stasyuk, O.A. Stasyuk, M. Solà, A.A. Voityuk, Electron Transfer in a Li^+-Doped Zn-Porphyrin–[10]CPP⊃Fullerene Junction and Charge-Separated Bands with Opposite Response to Polar Environments, J. Phys. Chem. B 124 (2020) 9095–9102.
[70] S. Zank, J.M. Fernández-García, A.J. Stasyuk, A.A. Voityuk, M. Krug, M. Solà, D.M. Guldi, N. Martín, Initiating Electron Transfer in Doubly Curved Nanographene Upon Supramolecular Complexation of C_{60}, Angew. Chem. Int. Ed. 61 (2022) e202112834.